Journal of Computational Physics **162,** 467–482 (2000)
doi:10.1006/jcph.2000.6550, available online at http://www.idealibrary.com on IDEAL®

Robust Numerical Simulation of Porosity Evolution in Chemical Vapor Infiltration I: Two Space Dimension

Shi Jin,*[,1] Xuelei Wang,* Thomas L. Starr,†[,2] and Xinfu Chen‡[,3]

**School of Mathematics, Georgia Institute of Technology, Atlanta, Georgia 30332; †Department of Chemical Engineering, University of Louisville, Lousville, Kentucky 40292; and ‡Department of Mathematics, University of Pittsburgh, Pittsburgh, Pennsylvania 15260*
E-mail: jin@math.gatech.edu, xwang@math.gatech.edu, tom.starr@louisville.edu

Received June 1, 1999; revised May 5, 2000

A numerical method is presented for describing pore structure evolution during chemical vapor infiltration densification and other physical problems of gas–solid reactions involving growth of a porous solid. Our method, based on the model proposed in (Jin *et al.*, 1997, J. Mater. Res. **14**, 3829), uses the level set equation of Eulerian formulation coupled with a boundary value problem of the Laplace equation. It allows robust numerical capturing of topological changes such as merging and formation of pores during the process. An efficient numerical method for the detection of the inaccessible pores is introduced for models in the kinetic limit, where the front speed is constant. Numerical examples show that this model will accurately predict not only the residual porosity, but also the precise close-off time, location, and shape of all pores.

1. INTRODUCTION

The chemical vapor infiltration (CVI) process is an important approach to fabricating ceramic matrix composites (CMCs). Two variations, isothermal CVI (ICVI) and forced flow-thermal gradient CVI (FCVI), are typically utilized. In CVI a vapor precursor of the matrix material, such as methyltrichlorosilane (MTS), diffuses through (in ICVI) or is forced (in FCVI) into a network of reinforcing fibers at elevated temperature. The MTS dissociates at the fiber surface and deposits silicon carbide (SiC), "growing" the solid fiber and filling

[1] Research was supported in part by NSF Grant DMS-9704957. Current address: Department of Mathematics, University of Wisconsin, Madison, WI 53706. jin@math.wisc.edu.

[2] Research supported by U.S. Department of Energy, Fossil Energy AR&TD Materials Program.

[3] Research was supported in part by NSF Grant DMS-9971043.

0021-9991/00 $35.00

the interfiber void. As matrix growth progresses, avenues for gas transport become more tortuous and begin to close off. Infiltration and matrix consolidation eventually cease when the pores no longer form a percolating network through the composites. Under optimum processing conditions (at the kinetic limit discussed above), the transport of MTS from the surroundings is rapid relative to the deposition rate and growth continues at a constant rate as long as there is a continuous path to the surrounding source of the precursor.

The CVI process is one example of a more general physical phenomena—gas–solid reactions involving porous solids where porosity of the porous medium diminishes as the volume of the solid phase increases. During the process, as described above, decreasing porosity makes it possible to form inaccessible pore space in the course of the reaction, and more space may become inaccessible to transport from outside of the porous medium as the reaction proceeds further. In percolation theory, the lowest porosity that permits percolation of a fluid through the pore space is often referred to as the percolation threshold of the solid. In this paper we refer to it as residual or final porosity, which is very important as this determines to a great extent the final microstructure of the composite.

As CVI is used for fabrication of composites of increasing size and complexity, modeling has been a key element and will be even more important in the development of the CVI process. Many mathematical models have been developed to describe the structure evolution and to simulate the growth of the matrix on fibers found in the CVI process. These models emphasize different aspects of the CVI process: transport properties are computed by means of a random walk simulation scheme [21], porosity is visualized by three-dimensional x-ray microtomography [7, 8], effective diffusivities are computed using a Monte Carlo simulation scheme [20], and other models compute the physical properties such as surface area per unit volume, gas permeability, or thermal conductivity [14]. Most of these models are explicitly or implicitly based on the pseudo-steady-state hypothesis [22]—the mass and momentum transfer is very rapid compared to changes in pore geometry. Stated in another way, the whole internal surface area of the solid is accessible to the reacting fluid at all porosity levels or inaccessible pore volume formation does not take place. The reason is, as pointed out in [22], that a description of the change of the pore structure and the surface area is the most difficult thing to determine in modeling the CVI process. Some models try to overcome this difficulty. For example, a network of pores of distributed size and length is used to present porous medium structure [15]; Starr's model [18] allows initial fibers to grow and overlap, which simulates the microstructure more appropriately. All these models involve mathematical complexity and do not capture the essential characteristics of structure evolution. They are still far from real-time simulation of the CVI process due to the lack of a framework for quantifying the structure of interconnected porosity and relating it to measurable processing parameters such as permeability and densification. We would also like to mention the paper [3], where a one-dimensional optimization problem in CVI was analyzed.

In [6] we presented a mathematical model for CVI that is based on a coupled system of a Hamilton–Jacobi (H-J) level set equation and a Dirichlet boundary value problem of the Laplace equation. The level set method is a successful phenomenological model in numerically computing front propagation problems that can naturally handle singularities and topological changes such as breaking and merging [11, 13]. However, in order to use the level set method one has to provide the front speed, which is nonlocal for the CVI process. We used a boundary value problem of the Laplace equation as an indicator of the accessibility of each pore from the outer boundary. More specifically, the sign of the solution to this Laplace equation is used to determine whether a particular part of the front

will grow or cease to grow. Using this Laplace equation is also physically natural since its solution plays the role of concentration or temperature. In the CVI process, the gas diffusion is much faster than the growth of the fiber, making the diffusion process essentially time-independent. This leads to the Laplace equation for concentration or temperature.

The objective of this mathematical model is to simulate the developing fiber–matrix microstructure in two or three dimensions without incorporating kinetic theory or percolation theory. This is a new approach to this problem. Numerically simulating the process will monitor the changing of geometry microstructure and porosity.

In this paper, we provide numerical discretizations of this model. In particular, we assume that the process is in the kinetic limit, where the front speed is constant unless around inaccessible pores. This limit can be achieved under optimal processing conditions. In such a case, the front speed does not depend on the specific value of the solution to the Laplace equation; rather, they only depend on its sign. We introduce a very efficient way to detect the accessibility of the front. Since only the sign of the Laplace equation is needed, our accessibility determination does not solve the Laplace equation directly; instead we only check the sign of its solution. At each time step this algorithm needs merely $O(N)$ operations for N grid points, and as the porosity decreases the number of operations also decreases. This efficient algorithm, coupled with the solution to the Hamilton–Jacobi equation, which is obtained using the second order scheme developed by Osher and Sethian [11], offers a fast and robust way to simulate the evolution of the pore structure.

A related but much simpler problem arises in modeling photolithography, which is etching via some light energy source [13]. In this problem, whether a piece of the etched surface grows depends on whether it exposes to the energy source. Thus the growth rate depends on a given directional vector. The CVI process is much more complex since the gas transports and diffuses around all possible directions.

This paper is organized as follows. In Section 2, we review the model by Jin *et al.* introduced in [6]. In Section 3 we first present the second order scheme by Osher and Sethian on the Hamilton–Jacobi equation and then introduce an efficient way for detecting inaccessible pores. A large variety of numerical examples are given in Section 4. We conclude in Section 5.

2. THE MATHEMATICAL MODEL

The qualitative behavior of the CVI process is described in Fig. 1. Consider, for example, an initial configuration of circular fiber fronts Γ that grow in the normal direction with a prescribed velocity c. The growth of the interface is caused by a chemical reaction with a mobile, gaseous reactant that diffuses from the outer boundary. As the fronts grow the neighboring fronts begin to interact and then merge. However, when three or more fronts interact they form an isolated pore (area denoted by O), which is inaccessible by reactant from the outer boundary $\partial\Omega$. Since the gas reactant cannot penetrate into these inaccessible pores, fronts surrounding these pores will stop growing. The final configuration is the domain filled with the fibers except for the isolated pores—the residual porosity that cannot be eliminated by further processing. For optimizing composite properties it is necessary to understand the relation between this residual porosity and the initial configuration of the fibers. This is particularly true for continuous filament composites where weaving and braiding processes offer a great opportunity to tailor the initial configuration of fibers.

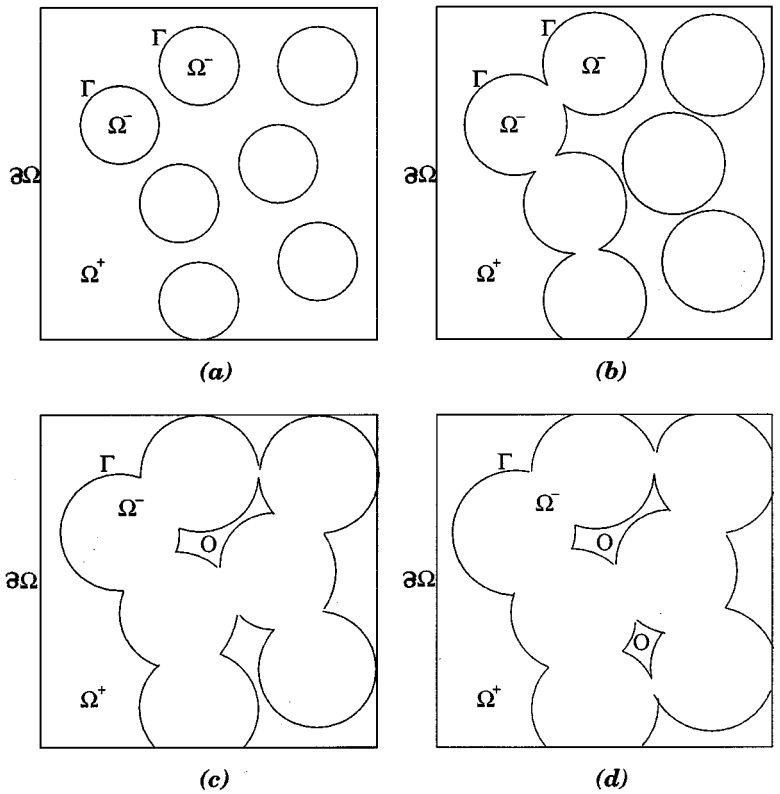

FIG. 1. Qualitative description of the CVI process. As front Γ grows, inaccessible pores (area O) form whose boundary ceases to grow.

In [6], a model based on the level set equation of Hamilton–Jacobi type, coupled with a boundary value problem of the Laplace equation, was introduced for such a process. Here we review this model.

Let $\phi(x,t)$ be the level set function, with zero level set as $\Gamma_t = \{x \mid \phi(x,t) = 0\}$. The initial choice of ϕ is arbitrary. For example, one can choose $\phi(x, t=0) = \pm d$, where d is the signed distance from point x to Γ_0, the initial fiber fronts. The plus (or minus) sign is chosen if the point x is outside (or inside) Γ_0—in the gas (solid) phase. The solid and gas phases are represented by $\Omega^- = \{(x,t) \mid \phi(x,t) < 0\}$ and $\Omega^+ = \{(x,t) \mid \phi(x,t) > 0\}$, respectively.

Now suppose the fibers' speed in the normal direction is $c(x,t)$, which may be a function of reactant kinetic (temperature, pressure, reactant concentration, etc.) or depend on local geometry such as the mean curvature. Then the zero level set of ϕ, which solves the following H-J equation [11],

$$\phi_t - c(x,t)|\nabla\phi| = 0\,, \tag{1}$$

describes the desired fiber surface propagating before inaccessible pores (area O) are formed. However, this equation cannot predict the formation of pores; thus the surface surrounding the pores will continue to grow with normal velocity c and eventually these pores will disappear just like the merging of two fronts. In order to correctly describe the behavior of the pores, we augment (1) with another equation satisfied by a concentration variable (or an order parameter for the pore) $u(x,t)$, defined in Ω^+, which solves the following

boundary value problem of the Laplace equation:

$$\begin{aligned} \Delta u &= 0 \qquad \text{in } \Omega^+(t), \\ u(x,t) &= 1 \qquad \text{on } \partial\Omega, \\ u(x,t) &= 0 \qquad \text{on } \Gamma_t\,. \end{aligned} \tag{2}$$

We then couple (1) and (2) by setting

$$\tilde{c}(x,t) = \begin{cases} c(x,t) & \text{if } u > 0, \\ 0 & \text{if } u = 0 \text{ and } \phi > 0. \end{cases} \tag{3}$$

The new level set equation is then

$$\phi_t - \tilde{c}(x,t)|\nabla\phi| = 0\,. \tag{4}$$

By the maximum principle for the boundary value problem of the Laplace equation [4], the solution of (2) satisfies $0 \le u \le 1$ on Ω^+, and the maximum value 1 and the minimum value 0 are attained only at the boundary $\partial\Omega$ and Γ. So before the formation of the pores, $0 < u < 1$ at all the interior points of Ω^+; thus every point at the front will propagate with normal velocity c. However, when the pore area O is formed, u defined in O has zero boundary condition on the boundary of O, which is part of Γ; thus the maximum principle implies that $u \equiv 0$ in O, which stops further shrinking of the pores, while in other parts of the front the growth speed remains c.

In summary, the solution of (2)–(4) gives the desired growth as described in Section 2.

Remarks.

1. The speed $c(x,t)$ can be any prescribed one, or any function of, for example, constant, local mean curvature, or other physical quantities.

2. In this model, just as in any front propagation described by the level set method, Γ can be any shape, while earlier models, such as that in [19], require the fibers to be circular.

3. In practice u may be defined in the whole domain Ω. In Ω^-, u will always be set to zero.

4. If the reactant input is only from part of $\partial\Omega$, then we can modify the boundary value of u from (2) accordingly.

5. The model remains the same in three dimensions, where all the fronts are surfaces.

3. NUMERICAL METHODS

3.1. *Numerical Method for the Hamilton–Jacobi Equation*

To solve the H-J equation (4), we use the second order scheme introduced by Osher and Sethian [11]. Let $D^{\pm}$ denote the finite difference operator

$$D^{+x}\phi \equiv \frac{\phi(x+h,t) - \phi(x,t)}{h}, \tag{5}$$

$$D^{-x}\phi \equiv \frac{\phi(x,t) - \phi(x-h,t)}{h}. \tag{6}$$

The scheme for (4) is described as

$$\phi_{ij}^{n+1} = \phi_{ij}^{n} + \Delta t[\max(\tilde{c}_{ij}, 0)\nabla^{+} + \min(\tilde{c}_{ij}, 0)\nabla^{-}], \tag{7}$$

$$\nabla^{+} = [\max(A, 0)^2 + \min(B, 0)^2 + \max(C, 0)^2 + \max(D, 0)^2]^{1/2}, \tag{8}$$

$$\nabla^{-} = [\max(B, 0)^2 + \min(A, 0)^2 + \max(D, 0)^2 + \max(C, 0)^2]^{1/2}, \tag{9}$$

where

$$A = D_{ij}^{-x} + \frac{\Delta x}{2} m\left(D_{ij}^{-x-x}, D_{ij}^{+x-x}\right), \tag{10}$$

$$B = D_{ij}^{+x} - \frac{\Delta x}{2} m\left(D_{ij}^{+x+x}, D_{ij}^{+x-x}\right), \tag{11}$$

$$C = D_{ij}^{-y} + \frac{\Delta y}{2} m\left(D_{ij}^{-y-y}, D_{ij}^{+y-y}\right), \tag{12}$$

$$D = D_{ij}^{+y} - \frac{\Delta y}{2} m\left(D_{ij}^{+y+y}, D_{ij}^{+y-y}\right), \tag{13}$$

where m is the minmod slope limiter function

$$m(x, y) = \begin{cases} \begin{cases} x & \text{if } |x| \le |y| \\ y & \text{if } |x| > |y| \end{cases} & \text{if } xy \ge 0; \\ 0 & \text{if } xy < 0. \end{cases}$$

3.2. *An Efficient Algorithm for Detecting Inaccessible Pores*

Solving a boundary value problem of the Laplace equation is complicated, especially for a complex geometry. If the front speed does not depend on the specific value but only the sign of u, such as in the kinetic limit, we only need the sign of the Laplace equation, which can be obtained rather efficiently using the method described below. The key observation is that, in the solution of the Laplace equation, u_{ij} in Ω^{+} is positive if u at one of the neighboring points has a positive sign. Here we propose a more efficient, $O(N)$, method, where N is the total number of grid points. This method defines all grid points in the accessible pore area Ω^{+} as $u = 1$ and other points as $u = 0$. Then we can simply define $\tilde{c}(x, t) = u(x, t) * c(x, t)$.

Let $B = \{(i, j) \mid u(i, j) = 1\}$ be the set of points in Ω^{+} that are accessible from the boundary $\partial\Omega$. Initially it contains only the boundary points where the reactant comes in. Starting with any points (i_1, j_1) from B, put its eight nearest neighboring points that belong to Ω^{+} but are not already in B (namely those at which $0 < u < 1$ and $\phi > 0$) into B by defining its value of u to be 1. Then go to the next neighboring point in Ω^{+} and repeat the previous procedure until all points in Ω^{+} at which $0 < u < 1$ have been checked.

At each time step, every point at Ω^{+} with a positive u value will be moved into B just once. Thus this algorithm needs at most $O(N)$ operations for each time step. In fact, at the later stage of the search when the residual porosity becomes small, the number of operations is far less than N since we only check into B the points in $\Omega^{+} - O$.

We now list the FORTRAN code for this fast algorithm. We use an indication function q for set B, namely, $B = \{(i, j) \mid q(i, j) = 2\}$.

First we include the code for the definition of the boundary points, which is used only at the first time step.

```
          KTOTALB=0
          DO 120 I=0,N
             IF(U(I,0,0).GT.ZERO)THEN
               Q(I,0)=2
               KTOTALB=KTOTALB+1
               X(KTOTALB)=I
               Y(KTOTALB)=0
             ENDIF
120       CONTINUE
```

The iterative search algorithm is given by (assume $(X(1), Y(1))$ is a boundary point):

```
            KTOTAL=KTOTALB
            LI=1
125         IL=X(LI)
            JL=Y(LI)
            DO 130 I=-1,1
            DO 130 J=-1,1
            IF((I.NE.0.OR.J.NE.0).AND.IL+I.GE.-1.
     *          AND.IL+I.LE.N+1.AND.JL+J.GE.-1.AND.JL+J.LE.N+1)THEN
               IF(Q(IL+I,JL+J).LT.2.AND.U(IL+I,JL+J,0).GT.ZERO)THEN
                 KTOTAL=KTOTAL+1
                 X(KTOTAL)=IL+I
                 Y(KTOTAL)=JL+J
                 Q(IL+I,JL+J)=2
               ENDIF
            ENDIF
130         CONTINUE
            LI=LI+1
            IF(LI.LE.KTOTAL)GO TO 125
```

From the description of the algorithm, we see that the total logic operation in calculating u is $O(N)$ at each time step, and this number decreases as the accessible porosity $\Omega^+ - O$ decreases.

Remarks:

(1) This algorithm checks the eight nearest neighbors for connectivity. In practice one can omit the check in the diagonal directions. This will speed up the computation at the cost of slightly lower accuracy.

(2) The process of filling a polygon in computer graphics is a process similar to detecting the accessible pores. See the flood fill algorithm in [1].

3.3. *Calculation of the Porosity*

We now discuss how the porosity is calculated numerically. The simplest way is to add the number of cells where $\phi > 0$ and divide it by the total number of cells. This is a first order calculation. To obtain a second order result, for each cell, we check the sign of ϕ on the four vertices. If they have the same (positive) sign, this cell will be counted as 1. If the sign changes, a linear interpolation is used to determine the location of zero of ϕ,

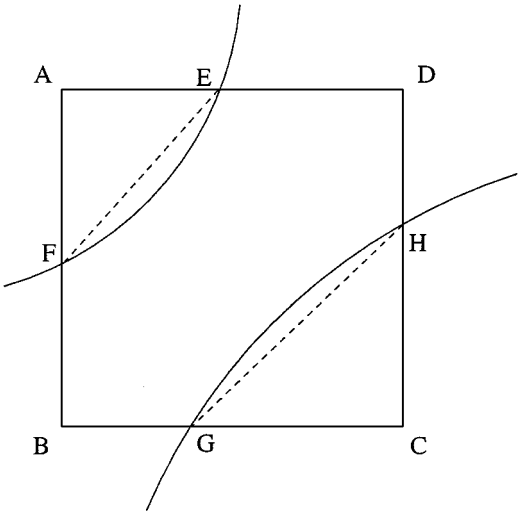

FIG. 2. Porosity calculation using linear interpolation.

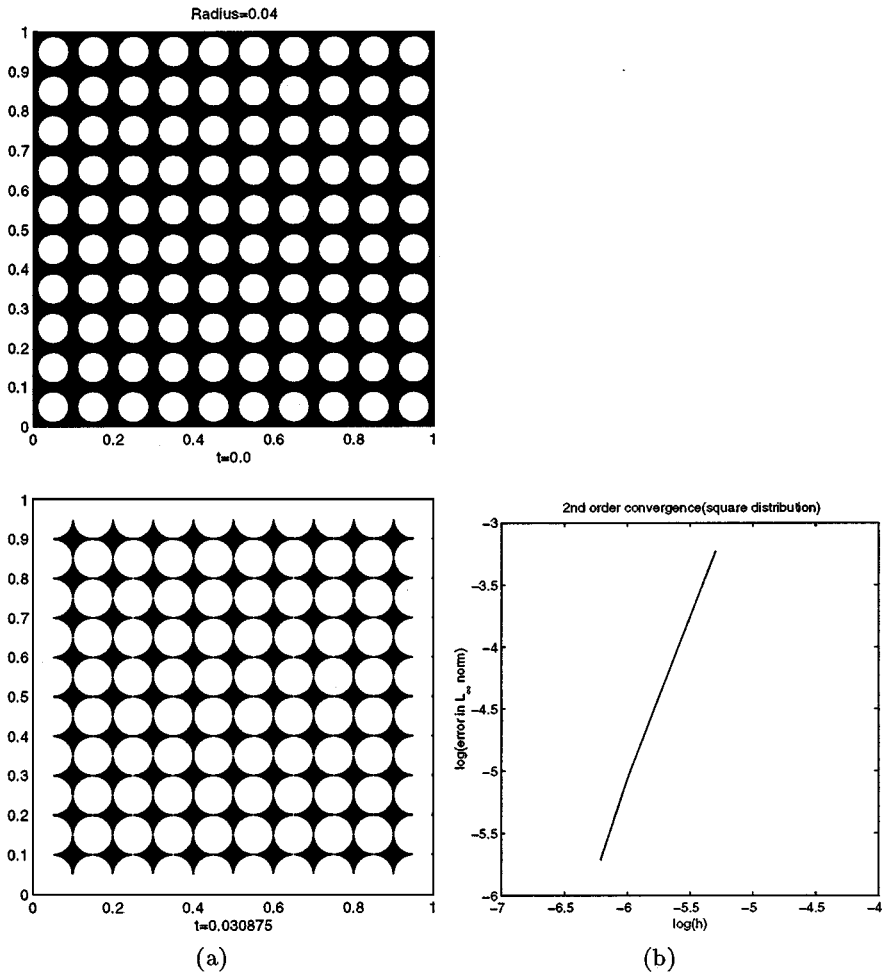

FIG. 3. (a) Square distribution and (b) second order convergence.

and this point is connected with the zero of ϕ on another side of the cell. The area of the corresponding polygon is then computed which gives the approximated porosity in that cell. An example is illustrated in Fig. 2, where one first finds the zeroes of ϕ at E, F, G, H, and then subtracts the areas of two triangles AEF and CGH from the area of square ABCD to obtain the porosity in this square.

4. NUMERICAL RESULTS

In this section we present some two-dimensional numerical experiments using the method presented in Section 3.

The computation is carried out over a 1×1 square box (except in the hexagonal distribution case, where the region is $1 \times \sqrt{3}$) with periodic boundary condition for ϕ, and in both space dimensions 300 grid points are used, with proper time step ($\Delta t = 1.25 \times 10^{-4}$)

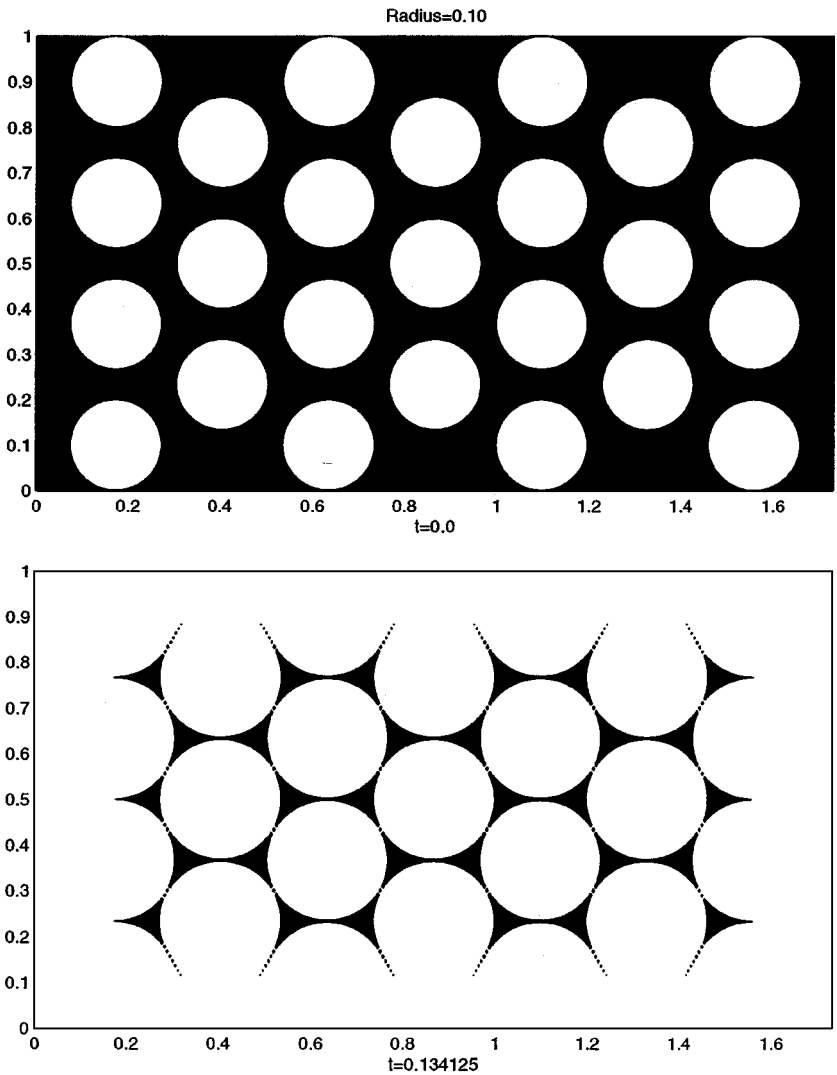

FIG. 4. Hexagonal distribution.

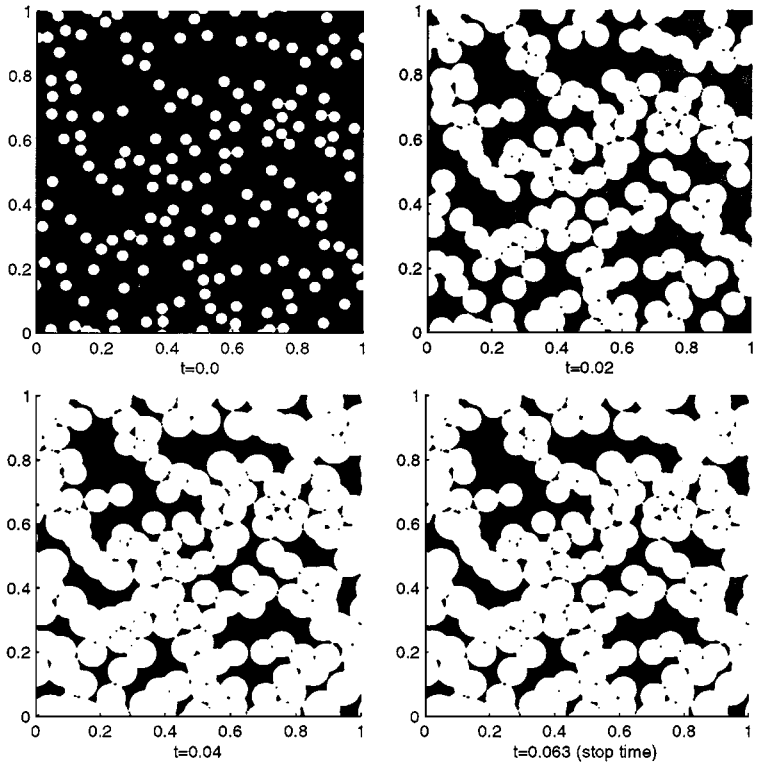

(a)

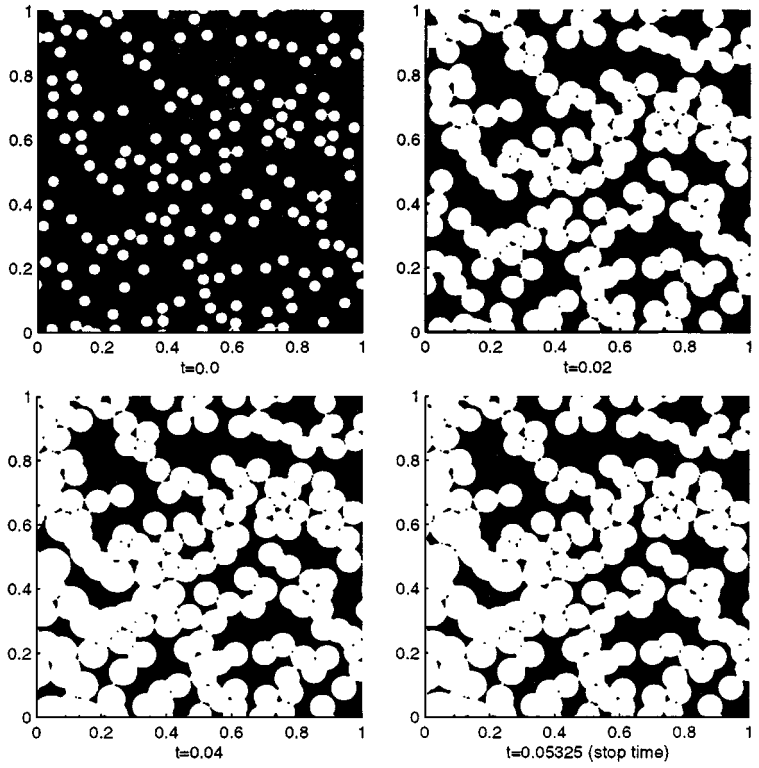

(b)

FIG. 5. (a) Random distribution I: inital porosity = 80%, source reactant comes from four sides of the boundary. (b) Random distribution II: inital porosity = 80%, source reactant comes only from left side of the boundary. (c) Instantaneous growth rate of porosity.

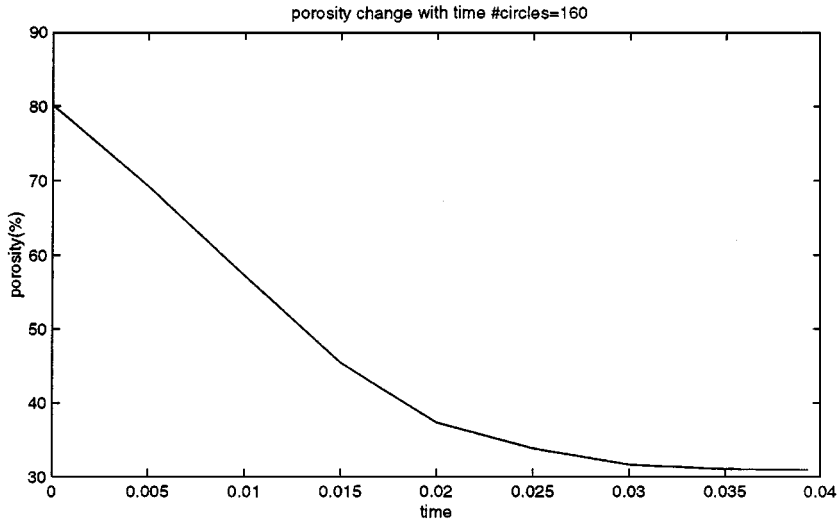

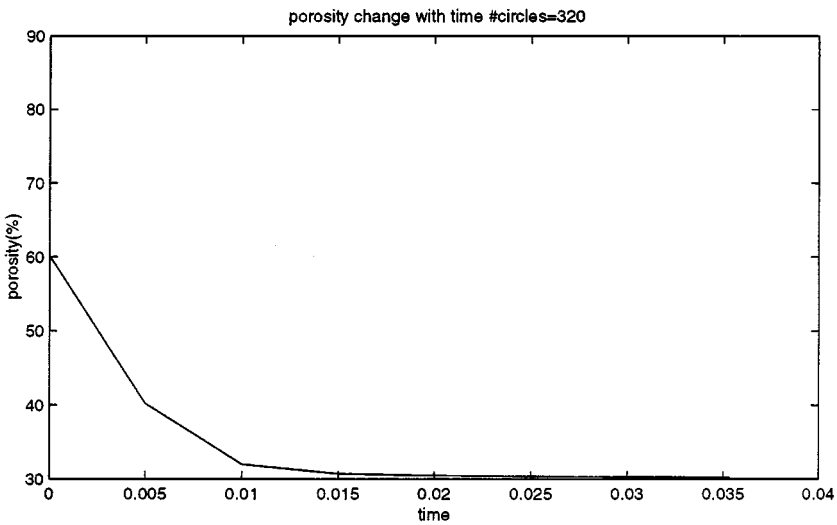

(c)

FIG. 5—*Continued*

satisfying the numerical stability condition. We test the model for the following cases of fiber distribution.

EXAMPLE 1 (Circles initially distributed on the square lattice). Monosized fibers are uniformly placed to form a square mesh. In this case the exact solution is known, which yields a final porosity $= 1 - \frac{\pi}{4} \doteq 21.46\%$. Our numerical experiment with the initial radius 0.04, as shown in Fig. 3a, yields the final porosity of 21.49%. This agrees with the exact solution very well.

To test the numerical accuracy of the scheme presented in Section 3.1 for the Hamilton–Jacobi equation in our application, we refine the mesh from the 100×100 discretization to the 500×500 one and calculate the error, defined as the difference of ϕ between every two consecutive runs during this refinement, in L_∞. In Fig. 3b the error versus the mesh size is plotted, which shows the second order accuracy.

TABLE I

Final Porosity When the Reactant Comes from Four Sides of the Boundary

Initial porosity	80%	70%	60%	50%
Average final porosity	25.29%	26.88%	27.20%	27.01%

EXAMPLE 2 (Circles initially distributed on a hexagonal lattice). Monosized fibers are uniformly placed to form a hexagonal mesh in a rectangle with height $\sqrt{3}$ and width 1. In this case the exact final porosity is also known, which equals $1 - \frac{\pi}{2\sqrt{3}} \doteq 9.31\%$. In Fig. 4, we show the numerical solution that begins with circles of radius 0.1. The final numerical porosity for this example is 11.24%. The slight loss of accuracy, compared with the first example, is due to the grid effect since in the first example the lattice is aligned with the spatial grid while in this one it is not. We then refine the mesh by a factor of 2 and obtain the final porosity 10.35%.

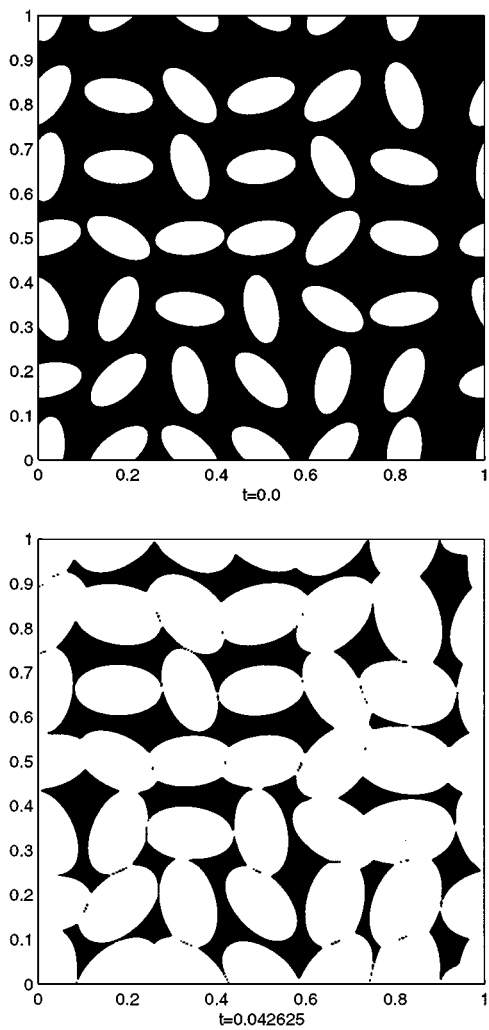

FIG. 6. Ellipses with random rotation.

TABLE II
Final Porosity When the Reactant Comes from the Left Boundary

Initial porosity	80%	70%	60%	50%
Average final porosity	33.34%	31.33%	30.00%	29.71%

EXAMPLE 3 (Circles of the same size randomly distributed initially). In Fig. 5a, we show the numerical simulation beginning with random initial distribution (no overlapping) of circles, with initial porosity of 80%. The gas reactant comes from all four sides of the boundary. In Fig. 5b we do the same simulation but assume the input boundary only at the left. To obtain an estimate of the relation between the initial porosity and the final porosity, we conduct experiments with random distributions of nonoverlapping circles of the same size with initial porosity 80, 70, 60, and 50%, respectively. For each initial porosity, we run ten different initial distributions and take the averaged final porosity. The results on the final porosity are given in Tables I and II.

In Fig. 5c we also plot the porosity versus time for both 160 and 320 circles in the case where gas is allowed from all four sides of the boundary. In both cases, one can see that the porosity decreases faster at the early stage and much slower toward the later stage.

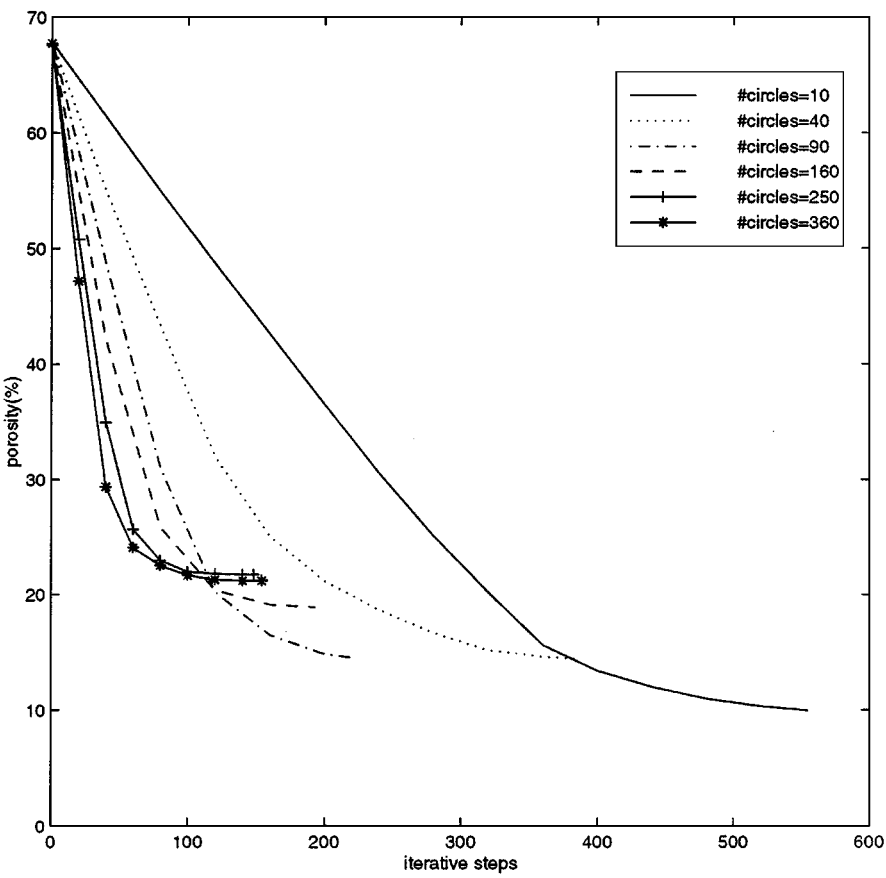

FIG. 7. The effect of the number of circles on instantaneous growth rate of porosity.

EXAMPLE 4 (Initial fibers of ellipse shape). The initial and equilibrium solutions are shown in Fig. 6. The example is to show that the model is suitable for fibers of any shape.

EXAMPLE 5. In this experiment, we are interested in how the number of circles (with fixed initial porosity) would affect the final porosity and computational time. We vary the radii of the initial circles, and consequently the number of the initial circles changes in order to have the same initial porosity. The radii we chose are $r_i = \frac{0.102}{i}$; thus the corresponding numbers of circles are $N_i = 10 \times i^2$, where $i = 1, 2, \ldots 6$. The initial porosity is $(1 - N_i \times \pi \times r_i^2) \times 100\% \doteq 67.31\%$ in all six cases. Initially, the circles are distributed randomly in a square region of unit size. We use a 300×300 uniform grid, and the time step is 2.5×10^{-4}. The computation stops when all pores are not inaccessible from any side of the boundary. We run each initial radius five times and find out the average for final porosity, total iterative steps, and CPU time. In Figs. 7 and 8, the porosity versus time, the number of iteration steps versus the initial number of circles, and the CPU time versus

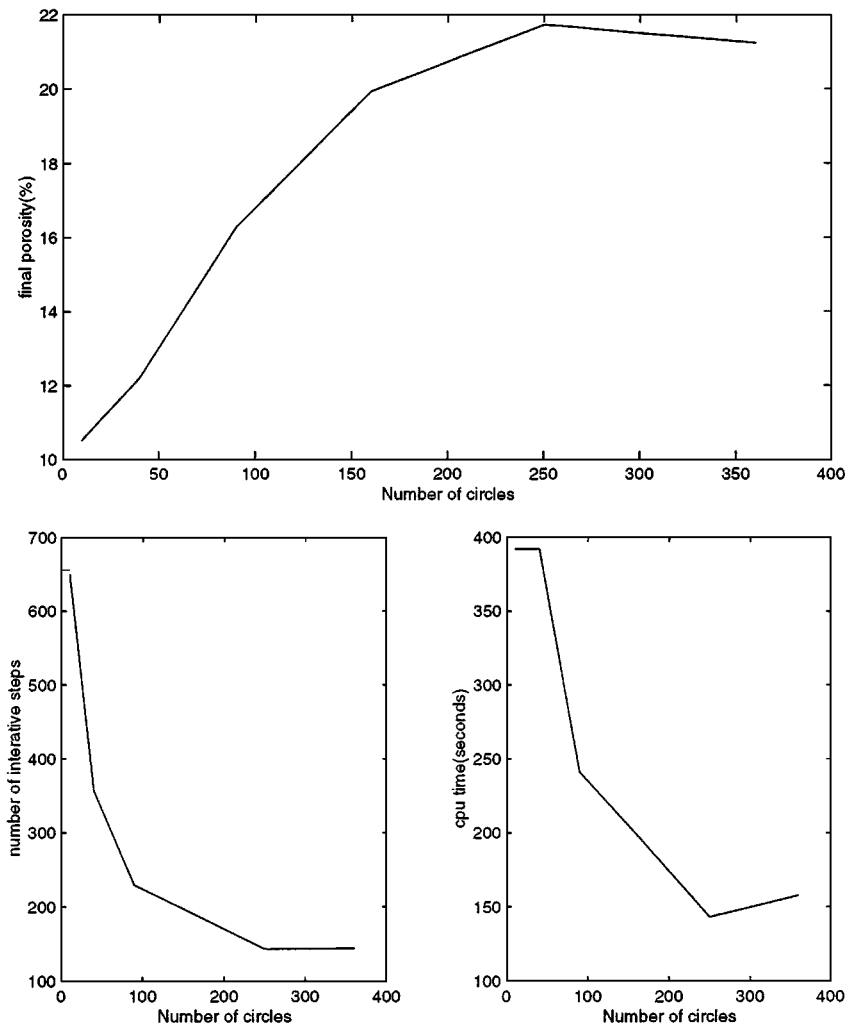

FIG. 8. The effect of the number of circles on final porosity, total iterative steps, and CPU time.

the initial number of circles are depictd. The experiment suggests that the fewer the initial number of circles is the smaller the final porosity is. This is not surprising—just imagine that if initially there is one circle the final porosity would be zero. However, one has to be concerned about the cost. As one increases the initial number of circles one reduces the number of iterations and the CPU time. Thus the optimal choice is the balance of final porosity and the production time, which is exactly the experience from the experiment.

5. CONCLUSION

In this paper we provide a robust numerical method for the simulation of the CVI process in composite fabrication under the kinetic limit, based on the model introduced in [6]. Our method, using the level set equation coupled with a boundary value problem of the Laplace equation, is an Eulerian formulation which allows robust treatment for topological changes such as merging and formation of pores without artificially tracking them. In the case of constant growth speed, we introduce an $O(N)$ algorithm to replace the Laplace solver, which allows us to identify the inaccessible pores in a very efficient way. Extensive numerical results show that the model precisely describes the desired growth property. As a result, it not only predicts the residual porosity, but also the precise locations and shapes for all pores.

In more realistic simulations the front speed may depend on the specific value or the gradient of the solution of the Laplace equation. In such a case we need to solve the Laplace equation in a complex geometry using some fast solver [9, 10, 12]. We leave this for a future paper. We will also couple the model with more physical properties, such as chemical reaction taking place at the interface and gas transport through the network, and apply them to many other physical problems where porosity plays a role.

ACKNOWLEDGMENTS

We thank the referees for their helpful comments.

REFERENCES

1. E. Angel, *Interactive Computer Graphics, a Top-down Approach with OpenGL,* 2nd ed. (Addison-Wesley, Reading, MA, 2000).
2. T. M. Besmann, B. W. Sheldon, R. A. Lowden, and D. P. Stinton, Vapor-phase fabrication and properties of continuous-filament ceramic composites, *Science* **253**, 1104 (1991).
3. H.-C. Chang, D. Gottlieb, M. Marion, and B. W. Sheldon, Mathematical analysis and optimization of infiltration process, *J. Sci. Comp.* **13**, 303 (1998).
4. L. C. Evans, *Partial Differential Equations* (Amer. Math. Soc., Providence, 1998).
5. J. Hoshen and R. Kopelman, Percolation and cluster distribution. I. Cluster multiple labeling technique and critical concentration algorithm, *Phys. Rev. B* **14**, 3438 (1976).
6. S. Jin, X. L. Wang and T. L. Starr, A model for front evolution with a non-local growth rate, *J. Mater. Res.* **14**, 3829 (1999).
7. J. Kinney, T. Breunig, T. Starr, *et al.*, X-ray tomogtaphic study of chemical vapor infiltration processing of ceramic composites, *Science* **260**, 789 (1993).
8. J. H. Kinney, C. Henry, D. L. Haupt, and T. L. Starr, The topology of percolating porosity in woven fiber ceramic matrix composites, *Appl. Comp. Mat.* **1**, 325 (1994).

9. R. J. LeVeque and Z. Li, The immersed interface method for elliptic equations with discontinuous coefficients and singular sources, *SIAM J. Numer. Anal.* **31**, 1019 (1994).
10. Z. Li, H. Zhao, and H. Gao, A numerical study of electro-migration voiding by evolving level set functions on a fixed cartesian grid, *J. Comput. Phys.*, to appear.
11. S. Osher and J. A. Sethian, Fronts propagating with curvature-dependent speed: algorithms based on Hamilton-Jacobi formulations, *J. Comput. Phys.* **78**, 12 (1988).
12. C. Peskin, Lectures on mathematical aspects on physiology, Lectures in Applied Mathematics **19**, 69–107 (1981).
13. J. A. Sethian, *Level Set Methods*, Cambridge Univ. Press, Cambridge, UK, 1996.
14. D. J. Skamser, D. P. Bentz, R. T. Covrdale, *et al.* Calculation of the thermal conductivity and gas permeability in a uniaxial bundle of fibers, *J. Am. Ceram. Soc.* **77**, 2669 (1994).
15. S. Sotirchos and S. Zarkanitis, A distributed pore size and length model for porous media reacting with diminishing porosity, *Chem. Eng. Sci.* **48**, 1487 (1993).
16. T. L. Starr, *Ceram. Eng. Sci. Proc.* **9**, 803 (1988).
17. T. L. Starr, Advances in modeling of the chemical vapor infiltration process, *Mat. Res. Soc. Symp. Proc.* **250**, 207 (1992).
18. T. L. Starr, Gas-transport model for chemical-vapor infiltration, *J. Mater. Res.* **10**, 2360 (1995).
19. S. Sotirchos and S. Zarkanitis, A distributed pore size and length model for porous media reacting with diminishing porosity, *Chem. Eng. Sci.* **48**, 1487 (1993).
20. M. Tomadakis and S. Sotirchos, Effective Knudsen diffusivities in structures of randomly overlapping fibers, *AIChE J.* **37**, 74 (1991).
21. M. Tomadakis and S. Sotirchos, Transport properties of random arrays of freely overlapping cylinders with various orientation distributions, *J. Chem. Phys.* **98**, 616 (1993).
22. S. Vaidyaraman, W. Lackey, P. Agrawal, and T. Starr, 1-D model for forced flow-thermal gradient chemical vapor infiltration process for carbon/carbon composites, *Carbon* **34**, 1123 (1996).